Histone H3K9 methylation promotes formation of genome compartments in *Caenorhabditis elegans* via chromosome compaction and perinuclear anchoring

Qian Bian[a,b,c,1], Erika C. Anderson[a,b,1,2], Qiming Yang[a,b], and Barbara J. Meyer[a,b,3]

[a]Department of Molecular and Cell Biology, University of California, Berkeley, CA 94720; [b]Howard Hughes Medical Institute, University of California, Berkeley, CA 94720; and [c]Shanghai Institute of Precision Medicine, Ninth People's Hospital, Shanghai Jiao Tong University School of Medicine, Shanghai, 200125, China

Contributed by Barbara J. Meyer, March 17, 2020 (sent for review February 4, 2020; reviewed by Steven Henikoff and John Lis)

Genomic regions preferentially associate with regions of similar transcriptional activity, partitioning genomes into active and inactive compartments within the nucleus. Here we explore mechanisms controlling genome compartment organization in *Caenorhabditis elegans* and investigate roles for compartments in regulating gene expression. Distal arms of *C. elegans* chromosomes, which are enriched for heterochromatic histone modifications H3K9me1/me2/me3, interact with each other both *in cis* and *in trans,* while interacting less frequently with central regions, leading to genome compartmentalization. Arms are anchored to the nuclear periphery via the nuclear envelope protein CEC-4, which binds to H3K9me. By performing genome-wide chromosome conformation capture experiments (Hi-C), we showed that eliminating H3K9me1/me2/me3 through mutations in the methyltransferase genes *met-2* and *set-25* significantly impaired formation of inactive Arm and active Center compartments. *cec-4* mutations also impaired compartmentalization, but to a lesser extent. We found that H3K9me promotes compartmentalization through two distinct mechanisms: Perinuclear anchoring of chromosome arms via CEC-4 to promote their *cis* association, and an anchoring-independent mechanism that compacts individual chromosome arms. In both *met-2 set-25* and *cec-4* mutants, no dramatic changes in gene expression were found for genes that switched compartments or for genes that remained in their original compartment, suggesting that compartment strength does not dictate gene-expression levels. Furthermore, H3K9me, but not perinuclear anchoring, also contributes to formation of another prominent feature of chromosome organization, megabase-scale topologically associating domains on X established by the dosage compensation condensin complex. Our results demonstrate that H3K9me plays crucial roles in regulating genome organization at multiple levels.

genome compartments | histone modifications H3K9me1/me2/me3 | chromosome compaction | perinuclear anchoring | gene expression

Eukaryotic genomes are organized into a series of higher-order structures within the 3-dimensional (3D) space of the nucleus (1–3). Chromatin loops can connect promoters of genes to distal regulatory elements located tens to hundreds of kilobases away (4, 5). In metazoans, topologically associating domains (TADs) of ∼1 Mb confine chromatin interactions to distinct genomic neighborhoods (6–9). The functional roles of TADs remain obscure (9–11), but TAD disruption by chromosomal rearrangements can cause transcriptional misregulation due to ectopic enhancer–promoter contacts (12–14). At an even higher scale, genomic regions preferentially associate with regions of similar transcriptional activity on the same chromosome and on different chromosomes, partitioning mammalian genomes into transcriptionally active (A) and inactive (B) genome compartments (15). Deciphering the molecular mechanisms underlying these hierarchical structural features is crucial for understanding the organization and regulation of genome functions.

Although active and inactive genome compartments are among the most prominent features of chromosome organization, the mechanisms that establish them remain elusive. Most loops and TADs can be eliminated by abrogating binding of key architectural proteins, including the SMC complex cohesin and the zinc-finger protein CTCF (16–19). However, genome compartments are preserved and enhanced in the absence of TADs, revealing that compartments are created through different mechanisms (20). The clustering of active and repressive genomic regions into separate compartments has been proposed to enhance transcriptional regulation and stabilize different expression states. However, the inability to perturb genome compartments has hindered our understanding of the functions of these higher-order chromatin structures.

Genome compartments correlate strongly with chromatin states in diverse organisms (21). In mammals, euchromatic regions form the A compartment and are characterized by active transcription and histone modifications, such as H3K4me3 and H3K27Ac. In contrast, heterochromatic regions form the B compartment and are characterized by transcriptional repression and the histone H3

Significance

Within nuclei, genomes are spatially partitioned into compartments of transcriptionally active and inactive chromatin. How compartments are formed and the functions these structures perform in gene regulation are not well understood. We show that heterochromatic histone modifications H3K9me1/me2/me3 play critical roles in establishing inactive Arm and active Center genome compartments in *Caenorhabditis elegans* via two distinct mechanisms. Anchoring of chromosome arms to the nuclear envelope via an H3K9me-binding protein promotes their *cis* association, thereby partitioning arms from center regions. An anchoring-independent mechanism compacts chromosome arms. Eliminating H3K9me modifications or disrupting perinuclear anchoring significantly weakens compartments. However, attenuation of compartments does not cause significant changes in gene expression. Our study demonstrates that chromatin modifications are important determinants of three-dimensional genome organization.

Author contributions: Q.B., E.C.A., and B.J.M. designed research; Q.B., E.C.A., and Q.Y. performed research; Q.B., E.C.A., and Q.Y. analyzed data; and Q.B., E.C.A., and B.J.M. wrote the paper.

Reviewers: S.H., Fred Hutchinson Cancer Research Center; and J.L., Cornell University.

The authors declare no competing interest.

Data deposition: The data reported in this paper have been deposited in the Gene Expression Omnibus (GEO) database, https://www.ncbi.nlm.nih.gov/geo (accession no. GSE144253).

[1]Q.B. and E.C.A. contributed equally to this work.

[2]Present address: Cardiovascular Research Institute, University of California, San Francisco, CA 94158.

[3]To whom correspondence may be addressed. Email: bjmeyer@berkeley.edu.

This article contains supporting information online at https://www.pnas.org/lookup/suppl/doi:10.1073/pnas.2002068117/-/DCSupplemental.

First published May 8, 2020.

modifications H3K9me2, H3K9me3, and H3K27me3. Existing evidence suggests two possible ways that chromatin marks could contribute to the formation of genome compartments. First, regions with matching chromatin marks could associate with each other. In a recent simulation study, the compartment organization observed in mammalian cells was best explained by a model in which interactions among heterochromatic regions are energetically favorable (22). The heterochromatic binding protein HP1, which recognizes H3K9me and undergoes phase separation, could drive associations between heterochromatin regions (23, 24). Second, positioning of heterochromatin at the nuclear periphery could promote separation of the genome into compartments. Heterochromatin marks are known to position genomic regions to the nuclear periphery to promote their interactions and compaction (25–27). Thus, heterochromatin-associated histone modifications and proteins may play a prominent role in genome compartmentalization.

However, the extent to which heterochromatic marks contribute to genome organization in metazoans has been challenging to evaluate experimentally. Eliminating either H3K9me or H3K27me3 in mice causes lethality, thereby impeding assessment of their functions in genome organization (28–30). Although centromere-proximal H3K9me-enriched heterochromatin in the filamentous fungus *Neurospora crassa* exhibits reduced interactions with surrounding euchromatin, partitioning of euchromatin from heterochromatin is more severely disrupted by loss of subtelomeric H3K27me2/me3 than H3K9me1/me2/me3 (31, 32), making the role of H3K9me unclear.

Here we use *Caenorhabditis elegans* as a model to investigate the roles of H3K9me in genome organization. The *C. elegans* genome has a unique distribution of repressive and active chromatin. The distal arms of all five autosomes and the left arm of the X chromosome form the inactive compartment and are enriched for the heterochromatin marks H3K9me1/me2/me3 and H3K27me3 as well as for repetitive DNA elements (27, 33, 34). The heterochromatic chromosome arms preferentially associate with nuclear lamina via the nuclear envelope protein CEC-4, which binds to H3K9me (35, 36). In contrast, the central regions of all chromosomes form the active compartment and are depleted for repressive chromatin marks. The central regions also exhibit a low level of lamina association and are enriched for actively transcribed genes.

C. elegans embryos lacking all forms of H3K9me are viable and develop to adulthood under normal growth conditions. Hence the worm provides a unique opportunity to explore the functions of H3K9me in a metazoan. Eliminating H3K9me by disrupting the histone H3K9 methyltransferases does derepress repetitive DNA elements in germlines of adults and does cause accumulation of RNA:DNA hybrids at high growth temperatures, ultimately leading to genome instability and sterility (37–39).

In addition to genome compartment architecture, *C. elegans* chromosomes are organized into megabase-scale TADs. Hermaphrodite X chromosomes have a unique TAD organization that distinguishes them from autosomes and the male X. Prominent, regularly spaced TADs on X are created by the dosage compensation complex (DCC), a condensin complex that represses transcription by half to equalize X expression between sexes (XO males and XX hermaphrodites) (40). TAD boundaries are defined by sequence-specific recruitment elements on X (*rex* sites) that promote high-occupancy DCC binding (10, 40). TAD boundaries are strengthened by enrichment of H4K20me1 on X caused by the H4K20me2 demethylase activity of a DCC subunit (41, 42), but roles of other histone modifications in TAD architecture are not known.

In this study, we used genome-wide chromosome conformation capture experiments (Hi-C) to quantitatively assess the impact of H3K9me on *C. elegans* genome architecture. Comparison of genome-wide chromatin interaction profiles in wild-type embryos versus *met-2 set-25* mutant embryos defective in H3K9 methyltransferases or *cec-4* mutant embryos defective in perinuclear anchoring revealed that H3K9me promotes formation of genome compartments through two different mechanisms. H3K9me-mediated perinuclear anchoring via CEC-4 regulates *cis*-association of chromosome arms, while anchoring-independent functions of H3K9me control chromosome arm compaction. In addition, H3K9me but not perinuclear anchoring facilitates formation of DCC-dependent TADs on X.

Although loss of H3K9me or disruption of perinuclear anchoring led to significant weakening of compartmentalization, no significant changes in expression were found for genes that switched compartments, suggesting that the compartment in which a gene resides is not a major determinant of its expression level. Furthermore, increased compartment intermingling in mutants did not cause dramatic expression changes for genes that remained in their original compartments. Although genes that remained in the inactive Arm compartment exhibited an up-regulation in *met-2 set-25* double and *cec-4* single mutants relative to genes that remained in the active Center compartment, the expression changes were caused primarily by local repressive effects of H3K9me. Therefore, genome compartment strength does not dictate levels of gene expression. Finally, loss of H3K9me, but not disruption of perinuclear anchoring, led to weakening of TAD boundaries established by the DCC on hermaphrodite X chromosomes. Our findings demonstrate an intimate relationship between histone modifications and genome organization that broaden our understanding of the determinants and functions of 3D genome architecture.

Results

H3K9me Regulates Genome Compartments in *C. elegans*. Our previous Hi-C results from mixed-stage embryos revealed that the two arms of all *C. elegans* autosomes preferentially associate with each other, both *in cis* and *in trans*, while the central regions of autosomes preferentially associate with each other *in trans* (40). The left arm of chromosome X associates with autosomal arms *in trans*, and the remainder of X associates with the central regions of autosomes. This segregation of large active Center and inactive Arm chromatin regions partitions the genome into two compartments, comparable to the active A and inactive B compartments observed in flies and mammals, thereby providing the opportunity to dissect the molecular basis of genome compartmentalization.

Further analysis of our genome-wide Hi-C data in wild-type *C. elegans* embryos (10, 40) revealed architectural differences among the different chromosomes (Fig. 1*A*). The two arms of the three smaller autosomes (chromosomes I, II, and III) interact *in cis* at a higher frequency than expected for loci at that distance (Fig. 1 *A* and *D*), while the arms of the larger autosomes (chromosomes IV and V), which are separated by longer central regions, do not exhibit elevated *cis* interactions (Fig. 1 *A* and *J*). The right arm of chromosome V exhibits a unique topology. The ∼3-Mb region at the distal end of chromosome V forms a well-defined subdomain (ArmD subdomain) that separates from the remainder of the right arm. In contrast, the more central ∼3-Mb region of the right arm (ArmC subdomain) does not exhibit strong self-association. Both ArmD and ArmC subdomains interact strongly with the center regions adjacent to the Arm–Center junction (Fig. 1*J* and *SI Appendix*, Fig. S1*G*).

To assess the role of H3K9me in *C. elegans* genome organization, we performed in situ Hi-C in embryos lacking functional MET-2 and SET-25 methyltransferases, the major enzymes that deposit H3K9me1/me2 and H3K9me3, respectively. The *met-2 set-25* mutant embryos have no detectable H3K9me of any form (27, 37). Comparison of genomic distance-normalized Hi-C interaction frequencies (Z-scores) between *met-2 set-25* mutant and wild-type embryos (Fig. 1 *A–C* and *SI Appendix*, Fig. S1 *A* and *B*) revealed several obvious changes in chromatin interactions that reflect a loss of compartmentalization in the absence of H3K9me. First, in the double mutant, the two distal arms of chromosomes I, II, and III interact less frequently *in cis* (Fig. 1 *D–F* and *SI Appendix*, Fig. S1 *D* and *E*). In contrast, arms of chromosomes IV and V, which exhibit less prominent *cis*–arm association in wild-type embryos, are less affected in *met-2 set-25*

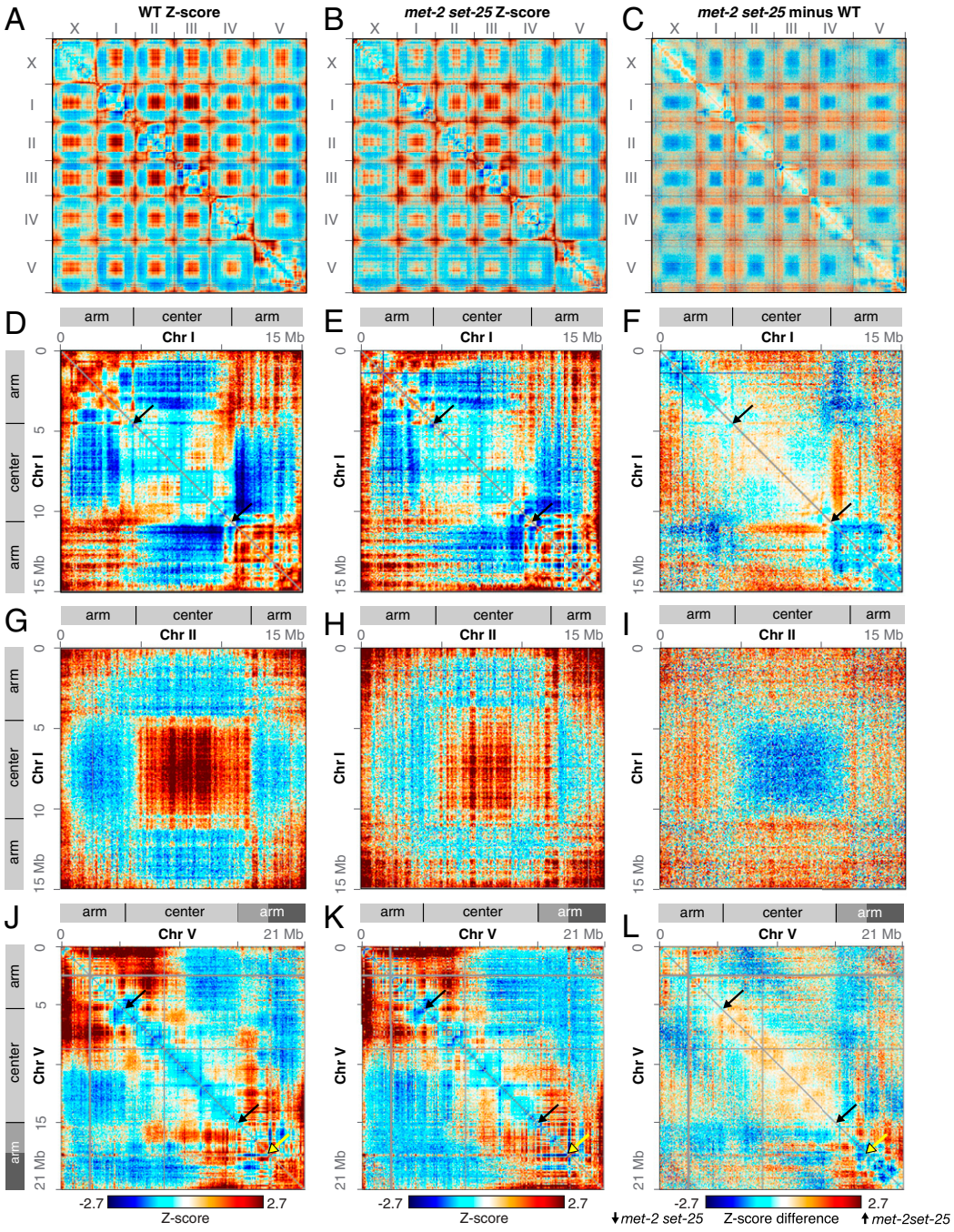

Fig. 1. Elimination of H3K9me weakens genome compartments. (*A* and *B*) Whole-genome heatmaps show Hi-C Z-scores for the X chromosome and autosomes I–V in wild-type and *met-2 set-25* mutant embryos. Red indicates higher interactions than expected for loci at a given distance, and blue indicates lower interactions than expected. The plaid pattern in interchromosomal interactions reflects compartment formation (high interactions between chromosome centers *in trans* and between chromosome arms *in trans*). (*C*) A Z-score subtraction heatmap shows increased (red) interactions between arms and centers and decreased (blue) interactions between centers and between arms in *met-2 set-25* mutant compared to wild-type embryos. (*D–F*) Chromosome I heatmaps show Hi-C Z-scores in wild-type and *met-2 set-25* mutant embryos and their difference. Diagrams delineate the Arm and Center compartments based on principal component analysis. Black arrows mark borders between Arm and Center domains. (*G–I*) Z-score heatmaps show *trans* interactions between chromosomes I and II in wild-type and *met-2 set-25* mutant embryos and their difference. (*J–L*) The Z-score heatmaps show that the right arm of chromosome V consists of two subdomains (ArmC, mid gray, and ArmD, dark gray) demarcated by yellow arrows. Interactions between the two subdomains are low in wild-type but increase in *met-2 set-25* mutant embryos. Black arrows mark borders between Arm and Center domains. All heatmaps are binned at 50 kb.

mutants (Fig. 1 *J–L* and *SI Appendix*, Fig. S1 *G* and *H*). Second, interactions among central regions of all chromosomes decrease significantly in the mutants (Fig. 1 *A–C* and *G–I*). Third, *cis* interactions between chromosome arms and central regions on chromosomes I, II, and III increase significantly, as do *trans* Arm–Center interactions among all chromosomes (Fig. 1 *D–I* and *SI Appendix*, Fig. S1 *D* and *E*). On the right side of chromosome V, the ArmD subdomain exhibits higher *cis*-interactions with both the central region and the ArmC subdomain (Fig. 1 *J–L* and *SI Appendix*, Fig. S1 *G* and *H*). Altogether, these changes

demonstrate that H3K9 methylation plays a critical role in regulating the formation or maintenance of genome compartments in *C. elegans*.

H3K9me-Mediated Nuclear Peripheral Anchoring Facilitates Compartment Formation. Disrupting perinuclear anchoring of chromosome arms while maintaining H3K9 methylation revealed that perinuclear anchoring is required for full separation of Arm and Center compartments. In *C. elegans*, H3K9me-enriched chromatin is anchored to the nuclear periphery by the chromodomain protein CEC-4, which localizes to the nuclear envelope and binds to all three forms of H3K9me. Prior studies showed that disrupting CEC-4 caused delocalization of chromosome arms from the nuclear periphery to the same extent as disrupting the H3K9 methyltransferases (36). To assess whether H3K9me's role in compartmentalization is due to perinuclear anchoring of chromatin, we performed Hi-C in *cec-4* mutant embryos (Fig. 2 *A*, *D*, *G*, and *J*). Comparison between Z-score heatmaps of *cec-4* mutant and wild-type embryos revealed distinct changes in chromatin interactions among all chromosomes in a fashion similar to those in *met-2 set-25* mutant embryos (Fig. 2 *B*, *E*, *H*, and *K* and *SI Appendix*, Fig. S1 *C*, *F*, and *I*). Thus, perinuclear anchoring via CEC-4 appears to facilitate genome compartmentalization (Fig. 2 *A–L* and *SI Appendix*, Fig. S1 *A*, *C*, *F*, and *I*).

However, disruption of compartment organization in *cec-4* mutants is less substantial than that in *met-2 set-25* mutants, as indicated by differences in chromatin interaction patterns between the two mutant strains (Fig. 2 *C*, *F*, *I*, and *L*). We quantified the strength of genome compartments in *cec-4* and *met-2 set-25* mutants using principal component analysis of Hi-C interactions. The first principal component (PC1), which is highly correlated with nuclear lamina association, defines the genome compartments in wild-type embryos. Genomic 50-kb bins with positive first eigenvector values are in the Center compartment, and bins with negative first eigenvector values are in the Arm compartment. In the *cec-4* and *met-2 set-25* mutants, PC1 still delineated Arm and Center compartments, and nearly 90% of the genomic bins remained in their original compartment (Fig. 3 and *SI Appendix*, Fig. S2 *A–D*). However, while PC1 explained 89% of the genome-wide variation in Hi-C interactions in wild-type embryos, it only explained 69% of the variation in *cec-4* embryos and 63% in *met-2 set-25* embryos, indicating the compartments were weakened. Hence, perinuclear anchoring activity of H3K9me accounts for a large proportion, but not all of its functions in genome compartmentalization.

In addition to causing increased mixing between compartments, loss of perinuclear anchoring led to increased interactions within the right arm of chromosome V, specifically between the ArmC and ArmD subdomains (Fig. 2*K* and *SI Appendix*, Fig. S1*I*). Interactions between ArmC and ArmD were not further increased in *met-2 set-25* mutant embryos (Fig. 2*L* and *SI Appendix*, Fig. S1*H*). Thus, perinuclear anchoring not only promotes partitioning of active and inactive chromatin, it also promotes partitioning of two domains with similar chromatin marks.

Loci that Switch Compartments Reside Near Compartment Borders. In both *cec-4* and *met-2 set-25* mutants, the ∼10% of loci that switched compartments tended to be near compartment borders (Fig. 3 *A* and *B* and *SI Appendix*, Fig. S2 *A–D*). In some cases, a TAD adjacent to a compartment border switched compartments as a unit (Fig. 3 *A* and *B*). For example, a TAD on the left side of chromosome V switched from the Center compartment to the Arm component (Fig. 3*A*). In addition, a TAD within the Arm compartment on the left side of chromosome X moved into the Center compartment in both *met-2 set-25* and *cec-4* mutants, shifting the compartment border (Fig. 3*B*). Furthermore, a broad region consisting of multiple TADs on the right side of chromosome X switched from the Center compartment to the Arm compartment in *met-2 set-25* mutants, greatly expanding the Arm compartment on X (Fig. 3*B*).

Because the topology of X is regulated by a DCC, which resembles condensin, we asked whether the DCC also regulates compartment organization on X. We examined compartment structure after depleting a DCC subunit (SDC-2) that is essential for DCC binding to X. Loss of SDC-2 causes elevated X expression, decompaction of X, and disruption of TAD structure. DNA corresponding to a TAD on the left of X in wild-type embryos switched from the Arm to the Center compartment, as in *met-2 set-25* mutants (Fig. 3*C*). Moreover, disrupting the TAD structure by deleting only the eight DCC binding sites (*8rexΔ*) at DCC-dependent TAD boundaries caused an intermediate change in the left Arm–Center border in which the eigenvector values approached 0, indicating the domain does not associate strongly with either the Arm or Center compartment (Fig. 3*C*). Together, these results indicate that compartment switching by depleting SDC-2 is not solely the consequence of disrupting DCC-dependent TAD boundaries; it also requires loss of DCC activity. Since DCC disruption does not affect the distribution of H3K9me3 (43), both DCC-dependent and H3K9me3-dependent mechanisms must regulate compartment organization on X.

Perinuclear Anchoring of H3K9me and Anchoring-Independent Functions of H3K9me Differentially Regulate Genome Organization. Our Hi-C results indicate that H3K9me regulates genome compartmentalization through two mechanisms: The CEC-4–dependent perinuclear anchoring of chromosome arms and a CEC-4–independent mechanism. To further delineate how the two mechanisms influence genome compartmentalization, we quantified the changes for different categories of chromatin interactions in both *met-2 set-25* and *cec-4* mutants and illustrated these changes in interaction strength using cumulative frequency plots.

Quantification of interactions within chromosome arms revealed that H3K9me promotes compartmentalization, in part, by facilitating compaction of chromosome arms through a mechanism that is independent of perinuclear anchoring. Loss of H3K9me in *met-2 set-25* mutants resulted in a dramatic decrease in interactions within each chromosome arm (intra-arm) for the smaller and more compartmentalized chromosomes I, II, and III (median intra-arm Z-score 1.09 for wild-type and 0.76 for *met2 set-25*) (Fig. 4*A*), indicating decompaction of chromosome arms. In contrast, the left arm of chromosome V and both arms of chromosome IV exhibited only a slight decrease in intra-arm interactions in *met-2 set-25* mutants (Fig. 4*C*), and the right arm of chromosome V exhibited a slight increase (Fig. 4*B*). In *cec-4* mutants intra-arm interactions for different chromosome arms were either maintained or elevated (Fig. 4 *A–C*). Thus, anchoring-independent functions of H3K9me, but not CEC-4–dependent perinuclear anchoring, compact chromosome arms.

The increases in intra-arm interactions upon disruption of CEC-4 (Fig. 4 *A–C*) can be attributed to increased flexibility of chromosome ends, as indicated by the more frequent interactions between the chromosome ends adjacent to the telomeres and the remainder of the chromosome arms (*SI Appendix*, Fig. S2 *E–G*). The phenomenon was most prominent at the right end of chromosome V, where the ArmD subdomain clearly gained interactions with the ArmC subdomain in *cec-4* mutants (Fig. 2 *B*, *J*, and *K* and *SI Appendix*, Fig. S2*G*). This inward looping topology was inhibited by the elimination of H3K9me in *met-2 set-25* mutants (Fig. 2*L* and *SI Appendix*, Fig. S2*G*).

Perinuclear anchoring of the two distal arms for the three smaller autosomes promoted long-range *cis*–arm interactions. In *cec-4* mutants, the *cis* arm-to-arm interactions on chromosomes I, II, and III decreased dramatically (median Z-score 1.43 for wild type and 0.84 for *cec-4*) (Fig. 4*D*). Chromosomes IV and V, which do not show enriched *cis* arm-to-arm interactions in wild-type embryos, were affected to a smaller extent (*SI Appendix*, Fig. S3*A*). Furthermore, interactions among chromosome arms of different autosomes (*trans* arm-to-arm) increased slightly in *cec-4* mutants (Fig. 4*E* and *SI Appendix*, Fig. S3*B*). Thus, for chromosomes I, II, and III, perinuclear anchoring brings the two arms of the same chromosome into closer proximity while spatially constraining each chromosome within its own territory,

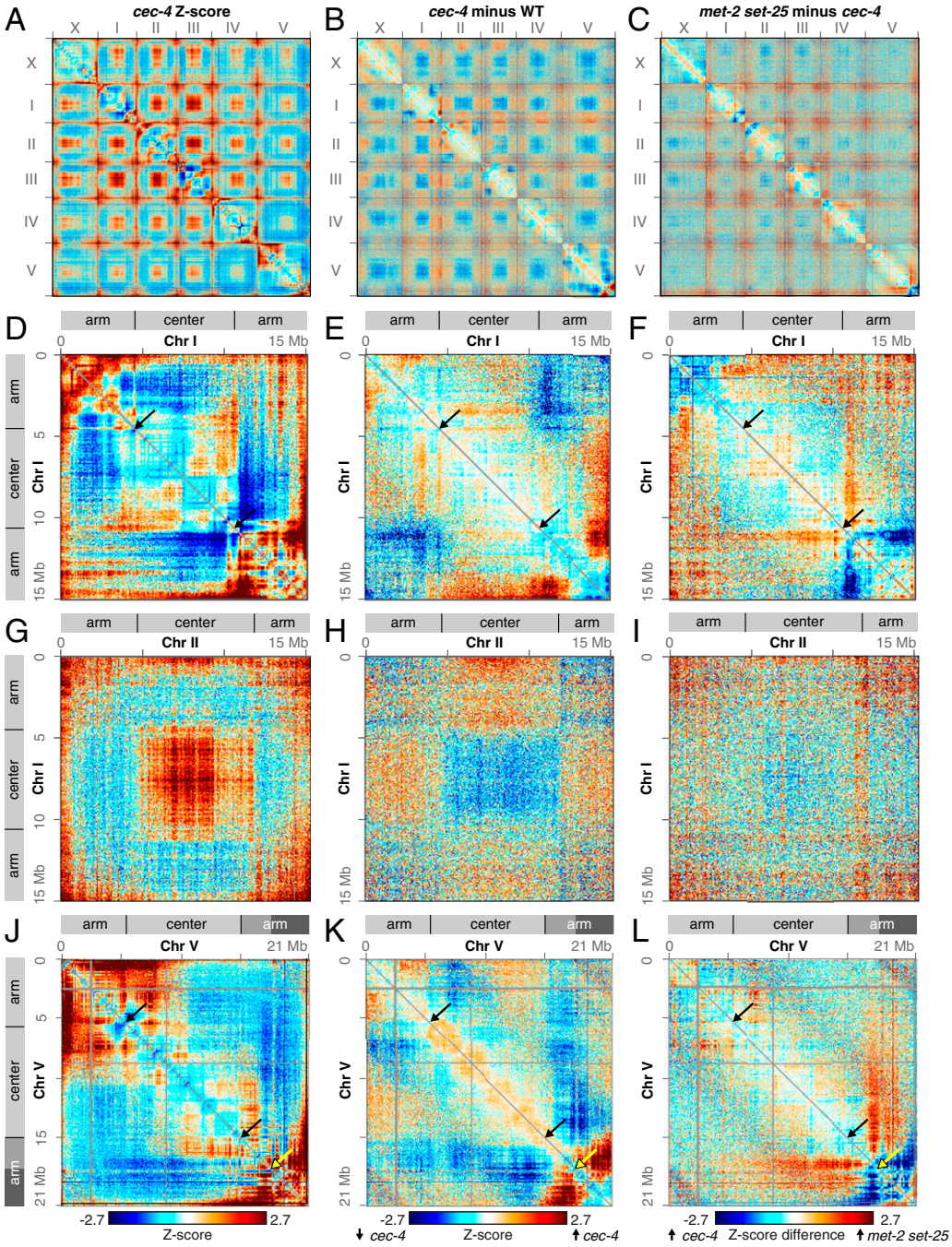

Fig. 2. Perinuclear anchoring of arms contributes to formation of genome compartments. (*A*) Whole-genome heatmap shows Hi-C Z-scores in *cec-4* mutant embryos, which lack anchoring of the H3K9me-enriched arms to the nuclear periphery. (*B*) Whole-genome Z-score subtraction heatmap shows increased (red) and decreased (blue) interactions in *cec-4* mutant compared to wild-type embryos. (*C*) Whole-genome Z-score subtraction heatmap shows increased (red) and decreased (blue) interactions in *met-2 set-25* compared to *cec-4* mutant embryos. (*D–F*) Chromosome I heatmaps show Hi-C Z-scores in *cec-4* mutant embryos and Z-scores in *cec-4* mutant compared to wild-type and *met-2 set-25* mutant embryos. Diagrams delineate the Arm and Center compartments based on principal component analysis. (*G–I*) The Z-score heatmaps show *trans* interactions between chromosomes I and II in *cec-4* mutant embryos and *cec-4* mutant compared to wild-type and *met-2 set-25* mutant embryos. (*J–L*) The Z-score heatmaps show that the right end of chromosome V strongly interacts with the rest of the right arm in *cec-4* mutant embryos. These interactions are greatly diminished in *met-2 set-25* mutant embryos. Black arrows mark borders between Arm and Center domains. Yellow arrows demarcate the boundary between the ArmC (mid gray) and ArmD (dark gray) subdomains. All heatmaps are binned at 50 kb.

creating a configuration that favors *cis* arm-to-arm interactions over *trans* arm-to-arm interactions.

Both *cis* arm-to-arm and *trans* arm-to-arm interactions increased in *met-2 set-25* mutants compared to *cec-4* mutants (Fig. 4 *D* and *E* and *SI Appendix*, Fig. S3 *A* and *B*), suggesting that decompaction of chromosome arms increases their chances of contacting other arms over long distance. Taken together, these results indicate that CEC-4–dependent perinuclear anchoring, but not anchoring-independent functions of H3K9me, promotes interactions *in cis* between the two arms of the three smaller autosomes to facilitate the formation of the Arm compartment.

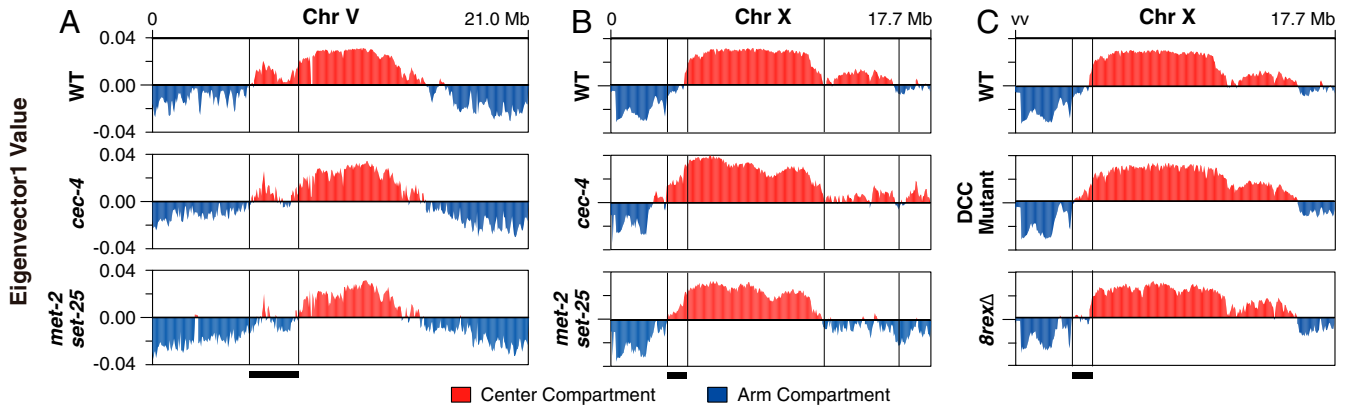

Fig. 3. Loci that switch compartments are near compartment borders. (*A* and *B*) Plots show eigenvector1 values for chromosomes V and X in wild-type, *cec-4*, and *met-2 set-25* mutant embryos. Positive values define the Center compartment and negative values define the Arm compartment. Some loci near compartment borders switch compartments. Black horizontal lines mark examples of TADs that switch compartments as a unit. (*C*) Eigenvector1 plots show that the same TAD on the left side of X that switches compartments in *cec-4* and *met-2 set-25* mutants also switches compartments in a DCC mutant (*Middle*). In *8rexΔ* (*Bottom*) the TAD exhibits an intermediate pattern, with eigenvector values closer to 0. The left vertical line for chromosome X is *rex-32*, which is deleted in *8rexΔ*.

Perinuclear anchoring of chromosome arms also dramatically affects interactions between chromosome arms and central regions. In *cec-4* mutants, arms of the three smaller autosomes interacted more frequently with the central region of the same chromosome (*cis* arm-to-center) (Fig. 4*G*). However, interactions between the right arm and center of chromosome V do not increase, likely due to the strong engagement between the right end of chromosome V with the rest of the chromosome arm (Fig. 2*K* and *SI Appendix*, Fig. S3*D*). In addition, loss of spatial constraints for chromosome arms in *cec-4* mutants enabled the arms of all chromosomes to gain interactions with central regions of different chromosomes (*trans* arm-to-center) (Fig. 4*H* and *SI Appendix*, Fig. S3*E*). Neither *cis* nor *trans* arm-to-center interactions were further increased upon elimination of H3K9me (Fig. 4 *G* and *H* and *SI Appendix*, Fig. S3 *D* and *E*), suggesting that perinuclear anchoring acts as the main inhibitor of intermingling between Arm and Center compartments.

Interactions within the central regions of all autosomes (intra-center) were minimally affected in both *cec-4* and *met-2 set-25* mutants, consistent with the paucity of H3K9me in the central regions (Fig. 4*F* and *SI Appendix*, Fig. S3*C*). However, interactions among central regions of different chromosomes (*trans* center-to-center) decreased in both *cec-4* and *met-2 set-25* mutants (Fig. 4*I* and *SI Appendix*, Fig. S3*F*), suggesting that the Center compartment can be influenced indirectly by loss of perinuclear anchoring of chromosome arms.

Compared to autosomes, compartmentalization of the dosage-compensated X chromosomes is less influenced by H3K9me. *Trans*-association between the central region of X and central regions of autosomes decreased in both *cec-4* and *met-2 set-25* mutants (*SI Appendix*, Fig. S3*L*), indicating some influence of H3K9me on X compartmentalization. However, changes in most other categories of interactions were minimal (*SI Appendix*, Fig. S3 *G–K*). These results, combined with the finding that DCC disruption alters the Arm–Center border on the left side of X (Fig. 3*C*), reinforce the view that both H3K9me-dependent and DCC-dependent mechanisms are required to achieve proper X compartment organization.

Altogether, our analysis of chromatin interactions revealed two tiers of genome organization imposed by different functions of H3K9me (Fig. 4*J*). The presence of H3K9me on chromosome arms leads to arm compaction independently of anchoring. The binding of H3K9me by CEC-4 anchors chromosome arms to the nuclear periphery greatly promotes the *cis*-association of arms in the shorter chromosomes I, II, and III, and prevents the intermingling of inactive Arm and active Center genomic regions. Perinuclear anchoring of the right arm of chromosome V also limits interactions between the end of the chromosome (ArmD subdomain) and the rest of the arm. The collective effects of H3K9me result in effective compartmentalization of the *C. elegans* genome.

Genes that Switch Compartments Do Not Show Significant Changes in Expression. Attenuation of Arm and Center compartments in *met-2 set-25* and *cec-4* mutants offered a unique opportunity to assess the role of genome compartmentalization in the regulation of transcription. In addition, our finding that *cec-4* mutants showed weakened genome compartmentalization, while retaining H3K9me levels allowed us to separate the global effect of genome compartmentalization from the local repressive effect of H3K9me.

We first explored whether the expression levels of genes that switched compartments changed to reflect their new compartment. Our analysis of published gene-expression datasets from *met-2 set-25* and *cec-4* young mutant embryos (36) revealed that only 3 of the 600 expressed autosomal genes that switched compartments in *met-2 set-25* mutants and none of the 332 autosomal genes that switched compartments in *cec-4* mutants showed significant (adjusted $P < 0.05$) changes in expression.

Although only rare individual genes exhibited a significant change in expression upon switching compartments, we tested the possibility that an entire set of genes that relocated into the active or repressive compartment might have significant changes in expression compared to those that remained in their original compartment. In *met-2 set-25* mutants, expression of the autosomal genes that switched from the repressive Arm compartment to the active Center compartment decreased slightly compared to genes that remained in the Arm compartment (Fig. 5*A*) ($P = 0.02$ for 134 genes, two-tailed *t* test), a trend opposite to that expected, while in *cec-4* mutants expression of the genes that switched from the Arm to the Center compartment increased only slightly (Fig. 5*B*) ($P = 0.03$ for 226 genes). Autosomal genes that switched from the Center to the Arm compartment in *met-2 set-25* mutants had no significant changes in expression (Fig. 5*A*) ($P = 0.15$ for 466 genes) compared to those that remained in the Center. In *cec-4* mutants, autosomal genes that switched from the Center to the Arm compartment had only a slight decrease in expression (Fig. 5*B*) ($P = 0.04$ for 106 genes). Therefore, genes that switch between active and repressive compartments do not assume the transcriptional status of their new compartment.

The converse was also found: The group of genes with significant changes in expression was not enriched for genes that switched compartments. Of 132 genes with significant expression

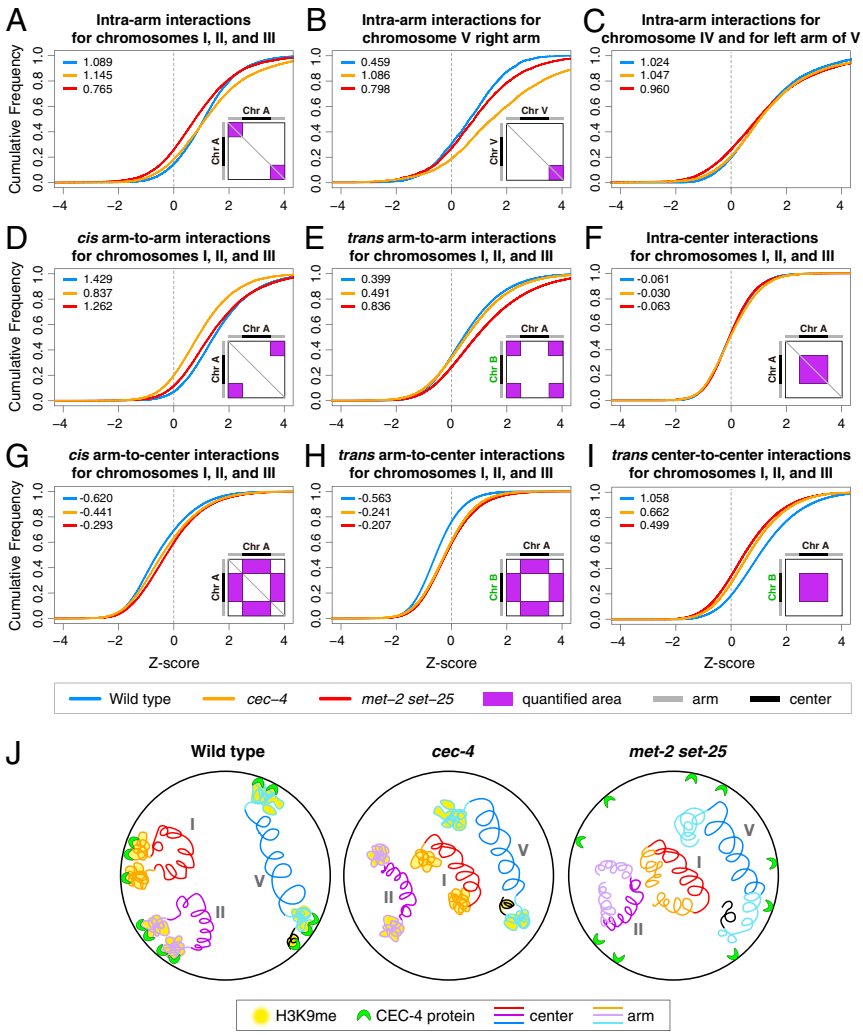

Fig. 4. Perinuclear anchoring and anchoring-independent functions of H3K9me in genome organization. (*A–I*) Cumulative frequency plots illustrate shifts in distribution of Hi-C Z-scores and changes in Z-score median values for different categories of interactions on chromosomes of wild-type, *met-2 set-25*, and *cec-4* embryos. Diagrams within the cumulative plots illustrate the quantified areas (purple) on the Z-score heatmaps for each interaction category. Schematics on the top and left of the diagrams depict chromosome arms (gray) and central regions (black). The median Z-score for each genotype is in the upper left corner of each plot. (*A–C*) In *met-2 set-25* but not *cec-4* mutants, the distribution of Z-scores for interactions within arms of chromosomes I, II, and III shifts leftward relative to that in wild-type embryos, indicating reduced interactions (*A*). Interactions within the right arm (*B*) but not left arm (*C*) of chromosome V increase dramatically in *cec-4* mutants. (*D*) *Cis* interactions between arms of chromosomes I, II, and III decrease more dramatically in *cec-4* than *met-2 set-25* mutants. (*E*) *Trans* interactions between arms of different chromosomes increase dramatically in *met-2 set-25* mutants. (*F*) Within the Center compartment, interactions within centers of chromosomes I, II, and III show no clear changes, while *trans* interactions between centers of different chromosomes dramatically decrease in both mutants (*I*). (*G*) *cis* and (*H*) *trans* interactions between arms and centers of chromosomes I, II, and III exhibit clear increases in both mutants, indicating increased intermingling between compartments. (*J*) The cartoons present a simplified view of how H3K9me likely controls compartmentalization through two mechanisms. For smaller autosomes I, II, and III, CEC-4-mediated perinuclear anchoring of chromosome arms brings the arms together. For chromosome V, perinuclear anchoring does not cause increased *cis*-association between arms, but limits interactions between the most distal region of the right arm (black) and the rest of the arm. In *cec*-4 mutants, the right end of V loops back internally. Independently of anchoring, H3K9me promotes compaction of arms. Compartment formation was not eliminated entirely in *met-2 set-25* mutants, implying that other mechanisms contribute to compartmentalization (see *Discussion*).

changes in *met-2 set-25* mutants (adjusted $P < 0.05$), none switched compartments. Only one gene had a significant expression change in *cec-4* mutants, and it did not switch compartments.

We also observed the same trends for X-linked genes, which we considered separately because they are subject to two different modes of chromosome-wide regulation. First, in both sexes genes on X are silenced in the germline, and this silencing is lost during early embryonic development. Second, starting in early embryonic development of hermaphrodites, genes on X are repressed twofold by the dosage-compensation process. As on autosomes, genes on X that switched between compartments in embryos of either mutant did not show changes in expression (Figs. 3*B* and 5 *A* and *B*) ($P > 0.5$).

Analysis of published gene-expression datasets from L1 larvae (44) revealed results similar to those observed in embryos. In general, autosomal and X-linked genes that switched between compartments in either of the L1 mutants were not significantly misregulated compared to genes that remained in the original compartments (*SI Appendix*, Fig. S4 *G* and *H*). An exception occurred for the 176 autosomal genes that switched from the active Center compartment to the repressive Arm compartment in *cec-4* mutants. They exhibited significant up-regulation, contrary to the expectation if the compartment dictated the level of gene expression. The L1 gene-expression data further corroborate the conclusion that the compartment in which a gene resides is not a major determinant of its expression level in *C. elegans*.

Relative Elevation in Arm Gene Expression Is Caused Primarily by Local Effects of H3K9me Rather than Compartment Intermingling. Using gene-expression data from young embryos, we assessed how expression of the genes that remained in their original compartment (90% of total expressed genes) was affected by loss of H3K9me2/me3 deposition and by loss of perinuclear anchoring. In *met-2 set-25* mutants, autosomal genes remaining in the Arm compartment were significantly more up-regulated than genes remaining in the Center compartment (Fig. 5*A*) ($P < 2.2 \times 10^{-16}$, two-tailed *t* test). In *cec-4* mutants, autosomal genes in the Arm compartment were also relatively elevated compared to genes in the Center compartment (Fig. 5*B*) ($P = 5 \times 10^{-5}$), although the differences were much smaller. Transcription of repetitive sequences was affected by loss of H3K9me (37, 38), but the inability to map repetitive reads uniquely prevented attribution of these changes to repeats in Arm versus Center compartments.

To understand the mechanisms underlying the relative elevation in Arm gene expression in mutants, we asked whether the elevation resulted from 1) loss of heterochromatic marks having local effects on genes with H3K9me peaks in wild-type embryos (45, 46), which are over-represented in Arm compartments (*SI Appendix*, Fig. S5 *A–C*), or from 2) increased compartment intermingling causing increased transcription throughout the Arm compartment. If the elevation of Arm gene expression was caused predominantly by impairment of a local H3K9me repressive function, we would expect genes associated with H3K9me in wild-type embryos, but not genes without H3K9me, to be up-regulated in mutants regardless of the compartment in which they resided. In contrast, if the increased compartment intermingling influenced gene expression, genes in the Arm compartment would be consistently more up-regulated than genes in the Center compartment, even when not associated with H3K9me. As shown below, the relative up-regulation of autosomal genes in Arm vs. Center compartments in mutants is generally better explained by a local repressive effect of H3K9me.

We categorized genes by their H3K9me2/me3 levels in wild-type embryos using chromatin immunoprecipitation sequencing (ChIP-seq) datasets (37) and then examined each category of genes for changes in expression (Fig. 5 *C* and *D*). Autosomal genes with H3K9me2 peaks in their promoter or gene body in wild-type embryos were significantly more elevated in expression in mutants than genes not associated with H3K9me2/me3 peaks (Fig. 5 *C* and *D*) for both Arm ($P < 10^{-13}$, *met-2 set-25* and $P < 10^{-13}$, *cec-4*, two-tailed *t* test) and Center ($P < 10^{-4}$, *met-2 set-25* and $P < 10^{-6}$, *cec-4*) compartments. These results indicate that H3K9me has a local repressive function in both Arm and Center compartments.

Repression occurs primarily for genes that have H3K9me2 in wild-type embryos but not for genes that have only H3K9me3 and no H3K9me2 (*SI Appendix*, Fig. S5 *D* and *E*), indicating a more critical role for H3K9me2 in repression. This finding is consistent with results of others examining repression of germline genes in embryonic somatic cells (46).

In *cec-4* mutants, the local repressive effects of H3K9me are sufficient to explain the up-regulation of genes. Autosomal genes with H3K9me2/me3 peaks showed similar increases in expression regardless of the compartment ($P = 0.95$), and genes without H3K9me2/3 showed similar decreases in expression regardless of the compartment ($P = 0.50$) (Fig. 5*D*). Therefore, increased compartment intermingling does not account for the relative up-regulation of Arm genes in *cec-4* mutants.

In *met-2 set-25* mutants, compartment-wide effects in addition to local repressive H3K9me effects contribute to the increase in Arm gene expression. Autosomal Arm genes in *met-2 set-25* mutants, unlike in *cec-4* mutants, were consistently elevated compared to Center genes, whether or not they had H3K9me2/me3 peaks in wild-type embryos ($P < 10^{-3}$ for all Center to Arm comparisons) (Fig. 5*C*). This compartment-wide effect cannot be attributed to increased intermingling between compartments because *met-2 set-25* mutants show a similar level of interactions between Arm and Center compartments as *cec-4* mutants (Fig. 4 *G* and *H*). Instead, the Arm up-regulation could result from long-range effects caused by decompaction of chromosome arms, which is observed in *met-2 set-25* but not *cec-4* mutants.

H3K9me, but Not Perinuclear Anchoring, Modulates DCC-Dependent TAD Organization on X Chromosomes. In addition to its role in compartment formation, H3K9me influences the formation of TAD boundaries on X chromosomes. Using a previously described, insulation-score approach (Fig. 6) (40), we found that the eight DCC-dependent TAD boundaries on X, but not the DCC-independent boundaries, were significantly weakened in *met-2 set-25* mutants (Fig. 6 *A* and *C* and *SI Appendix*, Figs. S1 *J* and *K* and S6 *E* and *F*). Boundaries that were completely eliminated in DCC mutant embryos were only weakened in *met-2 set-25* mutants (Fig. 6*G*), suggesting that H3K9me is necessary to reinforce but not create the boundaries.

In contrast, neither DCC-dependent nor DCC-independent TAD boundaries on X were significantly changed in *cec-4* mutants (Fig. 6 *B* and *D* and *SI Appendix*, Figs. S1*L* and S6 *A–F*). Therefore, our results suggest that the presence of H3K9me on X, but not the perinuclear anchoring activity of H3K9me, plays a significant role in regulating DCC-dependent TAD boundaries on X.

In addition to loss of DCC-dependent TAD boundaries, DCC-mediated interactions between strong *rex* sites were lost in *met-2 set-25* mutants but not in *cec-4* mutants. The interactions among the 25 highest DCC-occupied *rex* sites were significantly reduced in *met-2 set-25* mutant versus wild-type embryos, but not in *cec-4* mutant embryos (*SI Appendix*, Fig. S6*G*), further illustrating the interplay between the DCC and H3K9me, but not perinuclear anchoring, in shaping X-chromosome structure.

Although DCC-mediated TAD boundaries and *rex–rex* interactions require H3K9me, another DCC-mediated structure is retained in *met-2 set-25* mutants. The DCC promotes interactions between loci within 0.1 to 1 Mb, resulting in increased interactions on X compared to autosomes at that length scale (10). Unlike a mutant in which the DCC fails to assemble onto X, interactions within 1 Mb on X were unchanged in *cec-4* mutants (*SI Appendix*, Fig. S6*I*) and increased in *met-2 set-25* mutants (Fig. 6*H*).

The weakening of DCC-dependent TAD boundaries and *rex–rex* interactions in *met-2 set-25* mutants is not due to loss of DCC binding. Previous cytological studies showed neither *met-2 set-25* nor *cec-4* mutations prevented DCC binding to X (44). We further explored DCC occupancy by performing ChIP-seq for the DCC component SDC-3 (*SI Appendix*, Fig. S7) and also analyzed available ChIP-seq datasets (43) (*SI Appendix*, Fig. S7 *C* and *D*). Consistent with cytological studies, our DCC binding analyses show no significant changes in DCC occupancy at *rex* sites in either mutant (*SI Appendix*, Fig. S7), indicating that H3K9me modulates TAD boundary formation without affecting DCC binding to *rex* sites. We found no notable enrichment of H3K9me at or near the *rex* sites in published ChIP-seq datasets (34) (*SI Appendix*, Fig. S6*H*). Thus, H3K9me is not required for proper loading of the DCC. To regulate TADs, either a low level of H3K9me may be required at *rex* sites to facilitate TAD boundary formation, or H3K9me and its binding proteins could act distantly from *rex* sites to control TAD formation.

In contrast to the strong effects that *met-2 set-25* mutations have on DCC-dependent X TADs, almost no effects were found on autosomal TADs (Fig. 6 *E* and *F* and *SI Appendix*, Fig. S6 *A–C*). In both *met-2 set-25* and *cec-4* mutants, insulation profiles on autosomes were shifted, reflecting a change in chromatin compaction (*SI Appendix*, Fig. S2 *J* and *K*), but TAD boundary strength was unchanged (*SI Appendix*, Fig. S6 *B* and *C*) and TAD boundaries between Arm and Center regions were not weakened (*SI Appendix*, Fig. S6*D*). Our combined results reveal a role for H3K9me in regulating the formation of DCC-dependent TAD organization on X but not TAD organization on autosomes.

The up-regulation of X-linked genes in H3K9me mutants is not correlated with TAD organization. We plotted fold-changes of

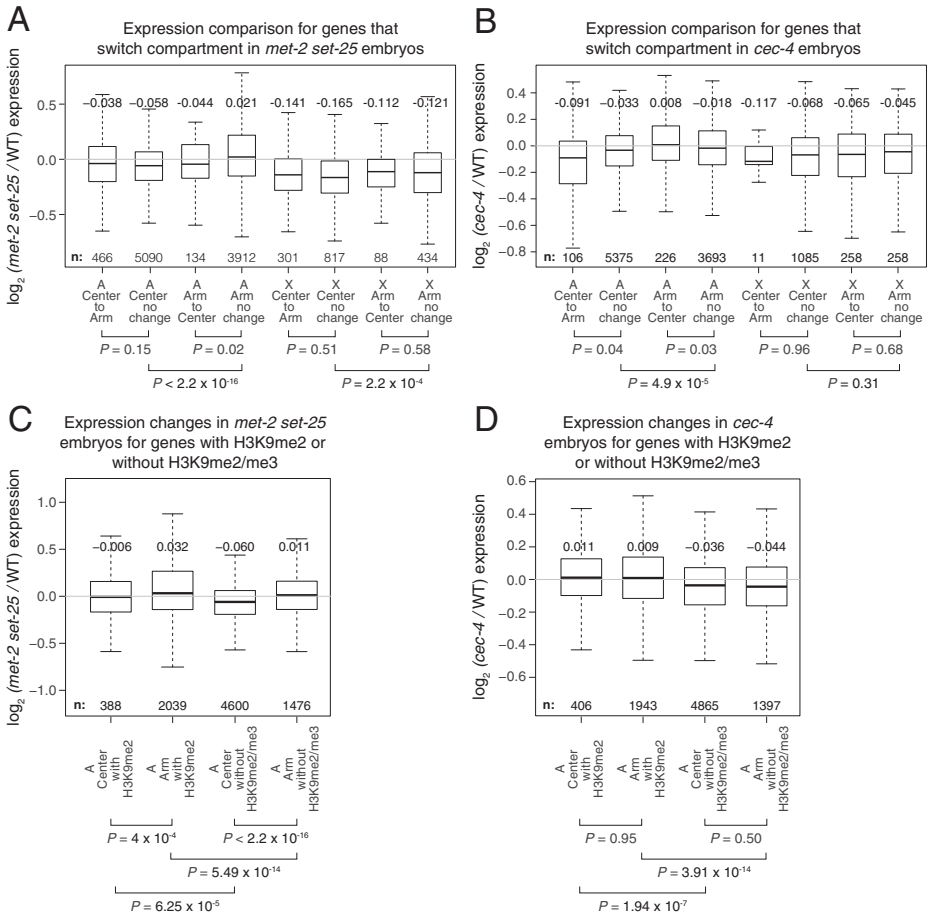

Fig. 5. Weakening of compartments does not cause significant changes in gene expression. (*A* and *B*) Box plot shows expression changes in *met-2 set-25* or *cec-4* mutant versus wild-type embryos for genes in Center and Arm compartments and genes that switch compartments on autosomes (*A*) and X. For each comparison, the median fold-change and number of genes included are listed. Genes with >1 fragment per kilobase of transcript per million mapped reads (FPKM) are included. Gene expression data are from ref. 36. (*C* and *D*) Box plots show early embryo expression changes in *met-2 set-25* or *cec-4* mutants for autosomal genes in Arm or Center compartments with H3K9me2 peaks (including those that also have H3K9me3 peaks) in the gene body or promoter, and with neither H3K9me2 nor H3K9me3 peaks. Genes with >1 FPKM that remain in the original compartment in mutant embryos are included. X-linked genes are excluded from analysis because of the small number of H3K9me2/me3 peaks. H3K9me2/me3 ChIP-seq data are from ref. 37.

gene expression in embryos and in L1 larvae along the genomic coordinates and found no discernible patterns of expression changes for X-linked (Fig. 6 *I* and *J* and *SI Appendix*, Fig. S4 *C*, *D*, *G*, and *H*) or autosomal genes (*SI Appendix*, Fig. S4 *A*, *B*, *E*, and *F*) relative to TADs in *met-2 set-25* or *cec-4* mutants. While only *met-2 set-25* mutant embryos exhibit substantial weakening of DCC-dependent TAD boundaries on X, both *met-2 set-25* and *cec-4* mutant L1 larvae (*SI Appendix*, Fig. S4 *G* and *H*) exhibit a similar magnitude of up-regulation along X. These results corroborate our earlier discovery that X-chromosome–wide gene repression is not coupled to DCC-driven TAD boundary formation (10).

Discussion

Our work has elucidated mechanisms that organize eukaryotic genomes into large-scale active and inactive chromatin compartments. Although patterns of histone modifications have been used to predict features of 3D genome architecture (47, 48), the roles played in genome organization by specific chromatin modifications, such as the heterochromatic modification of H3K9me, have been challenging to assess because of their essential roles in development. Here we show that H3K9me regulates genome organization in *C. elegans* by controlling the formation of transcriptionally active and inactive genome compartments on all chromosomes and by regulating the condensin-driven formation of TADs on X chromosomes.

Our analysis of chromatin interaction patterns caused by eliminating H3K9me revealed that this prominent heterochromatin mark regulates compartment formation in *C. elegans* through two distinct mechanisms. First, H3K9me promotes partitioning of inactive Arm from active Center compartments by regulating the radial positioning of chromosome arms. We showed that the perinuclear anchoring of H3K9me-enriched chromosome arms via chromodomain protein CEC-4 establishes a distinct chromosome configuration for the smaller autosomes by bringing the two distal arms of each chromosome into proximity. The larger autosomes IV and V do not exhibit such a CEC-4–dependent *cis* arm association, suggesting the size of central regions may present a topological barrier for the two arms to interact. However, for chromosome V, CEC-4–dependent perinuclear anchoring does modulate chromosome arm conformation by constraining interactions between subdomains within the right arm. Anchoring of the ArmD subdomain obstructs interactions between ArmD and the remainder of the arm, resulting in a more extended right arm conformation. For all autosomes, the spatial confinement of chromosome arms to the nuclear periphery promotes the separation between heterochromatic arms and euchromatic central regions, while strengthening interactions among central regions and thereby enhancing genome compartmentalization.

A recent cytological study of chromosome configuration suggested that CEC-4–dependent perinuclear anchoring influences genome organization differently in early-stage *C. elegans* embryos

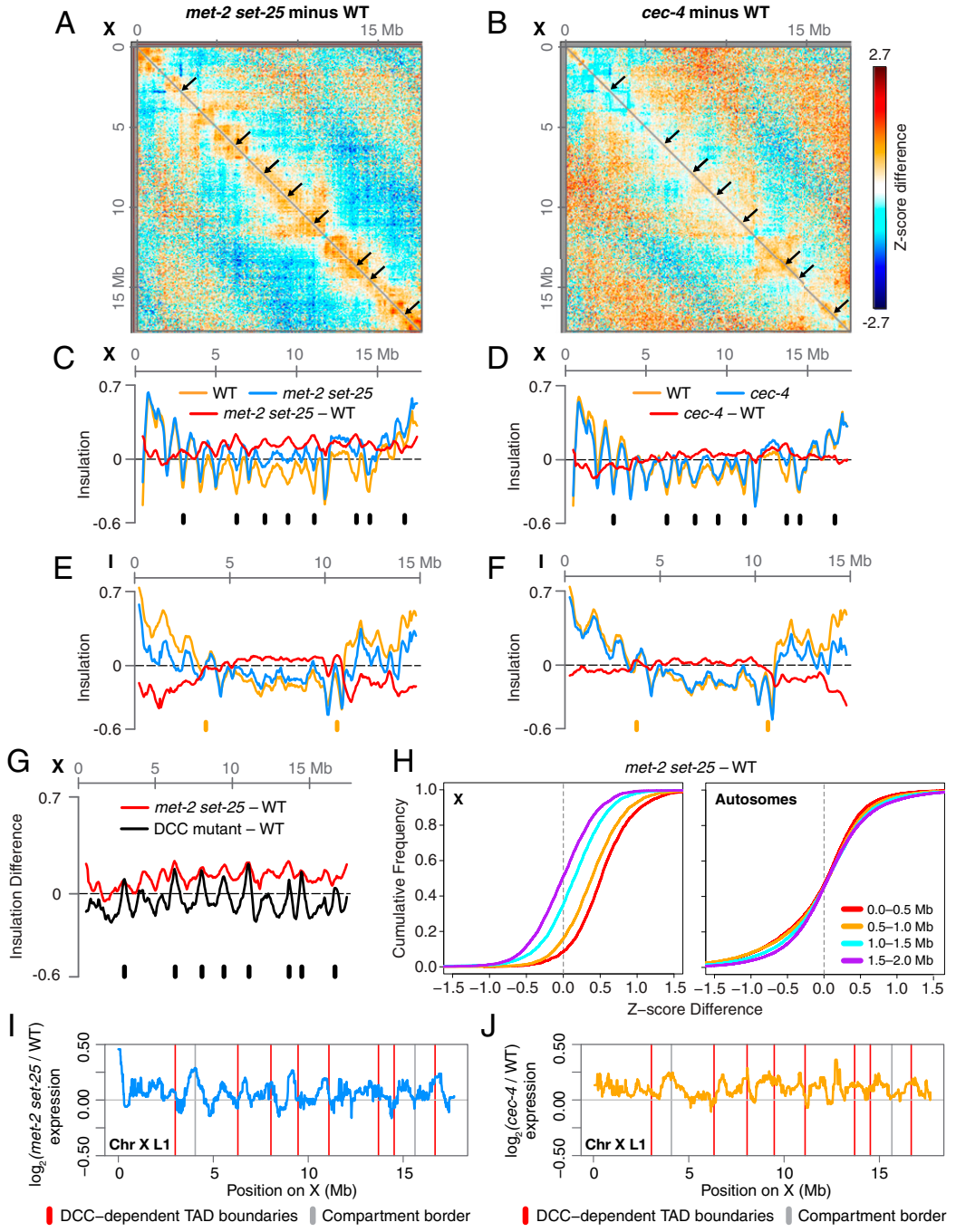

Fig. 6. Loss of H3K9me weakens DCC-dependent TAD boundaries on X. (*A* and *B*) X chromosome heatmaps binned at 50 kb show increased (red) or decreased (blue) Hi-C Z-scores in *met-2 set-25* or *cec-4* mutant compared to wild-type embryos. Black arrows mark DCC-dependent TAD boundaries. (*C*–*F*) Insulation plots show insulation scores across chromosome X or I in *met-2 set-25* or *cec-4* mutant (blue) and wild-type embryos (orange) and the insulation score difference between genotypes (red). Insulation profiles were generated by aggregating the interactions within a 500-kb window across every genomic interval. Local minima correspond to TAD boundaries, and the insulation differences between the minima at the boundaries and the maxima in the neighboring regions indicate the strength of the boundaries. Black ticks mark the position of DCC-dependent TAD boundaries. Orange ticks mark the position of borders between Arm and Center compartments. (*G*) X chromosome insulation plot shows the difference in insulation scores between either *met-2 set-25* mutant or the DCC mutant *sdc-2(y93, RNAi)* and wild-type embryos. TAD boundaries lost in the DCC mutant (black ticks) are weakened to a lesser extent in *met-2 set-25*. DCC mutant data are from ref. 10. (*H*) Cumulative plots show Z-score differences between *met-2 set-25* and wild-type chromosomes at different length scales. On X, interactions within a 1.5-Mb increase in *met-2 set-25* compared to wild-type embryos, while autosomal interactions are unchanged. (*I* and *J*) Median gene expression changes in *met-2 set-25* (blue) or *cec-4* (yellow) mutant L1s versus wild-type L1s in a 200-kb sliding window across chromosome X. Boundaries between Arm and Center compartments are marked with gray vertical lines. DCC-dependent TAD boundaries on X are marked with red vertical lines. Gene expression data come from ref. 44.

versus later-stage embryos in our study (49). Prior to gastrulation, perinuclear anchoring of chromosome arms led to an extended chromosome configuration, with low interactions between the two distal arms. Upon gastrulation, *cis* associations between arms increased, and a conventional Arm/Center compartment configuration emerged, as seen in our Hi-C studies. Changes that occur during embryogenesis may underlie the differential effects caused by CEC-4 at different stages of development, including the

maturation of constitutive heterochromatin, extended duration of cell cycle, and decrease in nuclear volume.

The second way H3K9me facilitates compartment formation is by promoting intra-arm chromatin interactions and thereby increasing compaction of chromosome arms. This process does not require CEC-4–dependent perinuclear anchoring. Clustering and compaction of heterochromatin in *Drosophila* is achieved by HP1α, the major binding protein of H3K9me, which forms phase-separated condensates in vitro and in vivo (23, 24). Such phase separation of heterochromatin could underlie aspects of genome compartmentalization in *C. elegans*.

Organization of the genome into Arm and Center compartments was not entirely eliminated in the absence H3K9me (Fig. 1*B* and *SI Appendix*, Fig. S1*B*). Thus, H3K9me-independent mechanisms also contribute to the formation of genome compartments in *C. elegans*. In the case of X, we showed that the DCC also contributes to defining compartment borders. In *N. crassa*, the heterochromatin mark, H3K27me2/me3, promotes intra- and interchromosomal interactions between subtelomeric heterochromatin (32), supporting the idea that multiple heterochromatin marks may collectively drive the association of heterochromatin regions. In *Drosophila*, interactions between actively transcribed genes that form the active A compartment are reduced upon inhibition of transcriptional elongation, suggesting that RNA polymerase II or other factors that bind active chromatin also contribute to compartment formation (50).

The functional significance of genome compartmentalization in the regulation of transcription had not been explicitly defined. In mouse and *Drosophila* cells, disruption of nuclear lamina results in increased intermingling between active and inactive compartments, detachment of a subset of lamina-associated domains from the nuclear periphery, and up-regulation of genes within lamina-associated domains (51, 52). However, lamina disruption also affects the chromatin association of many transcription regulators, such as histone deacetylases (53). Whether the observed gene-expression changes are caused by overall changes in genome architecture or instead the loss of chromatin-associated factors has not been resolved in these cases. Furthermore, many genomic regions switch between A and B compartments during differentiation of mammalian stem cells (54, 55). A subset of genes that switch compartments exhibit changes in expression that match the identity of the new compartment, although the correlation is modest. Mechanisms underlying these changes in expression are not known.

In this study, while the defects in H3K9 methylation or H3K9me-dependent perinuclear anchoring significantly weakened genome compartmentalization, they did not cause dramatic changes in gene expression in either active or inactive genomic compartments. With rare exception (3 of 932), genes that switched compartments did not show significant changes in expression. However, mild changes in expression were found for an entire set of genes that remained in its original compartment, with Arm genes exhibiting a relative up-regulation compared to Center genes. These changes in gene expression are attributable primarily to the impairment of a local H3K9me-repressive function, rather than to increased intermingling of inactive Arm and active Center compartments. In our experiments, eliminating H3K9me does not abolish compartments entirely and causes only 10% of the genome to transition between compartments. Hence, the possibility remains that complete disruption of genome compartments could cause more dramatic changes in gene expression.

In line with our results, the widespread transcriptional response triggered by heat shock was not accompanied by changes in A/B compartments in human or *Drosophila* cells (56), suggesting that compartment changes are not required for gene-expression changes. These findings support the view that the transcriptional status of a compartment, either active or inactive, does not play a deterministic role in setting the level of gene expression.

Although eliminating H3K9me in *C. elegans* causes minimal changes in expression of nonrepetitive genes in somatic cells, it does lead to significant derepression of repetitive elements in both the germline and soma, resulting in genome instability (37). A critical role for H3K9me in silencing repetitive elements and immobilizing transposons has also been observed in fission yeast, flies, and mammals (57–59). Whether the role of H3K9me in promoting genome compartmentalization has functional relevance for its conserved role in ensuring genome stability and genome defense is yet to be determined.

In addition to discovering functions for H3K9me in driving genome compartmentalization, we observed that H3K9me plays an unexpected role in regulating TAD organization. The *C. elegans* DCC, which includes a condensin subcomplex, induces formation of prominent TADs on X chromosomes. Current data suggest the DCC drives TAD formation through a loop-extrusion mechanism (10), as has been proposed for TAD formation in mammals (3, 20, 60, 61). Accordingly, the condensin subunits serve as the loop extruder whose extrusion activity is halted when the entire DCC binds to its highest-occupancy binding sites on X. The observed weakening of DCC-dependent TAD boundaries and decreased interactions between TAD boundaries in the absence of H3K9me are consistent with impaired functioning of the extrusion barriers. Curiously, although this study of H3K9me and our previous study of H4K20me (41) showed that the strength of DCC-dependent TAD boundaries is dependent on specific histone modifications, we found that H3K9me and H4K20me are enriched on chromosome arms or across X, respectively, rather than simply being enriched at the strong DCC-binding sites (*rex* sites) that define TAD boundaries. These findings, together with reports that TAD boundaries are disrupted in mammals by DNA methylation at specific CTCF binding sites that serve as loop extrusion barriers (62), suggest that TAD organization is subject to intricate regulation through both DNA and histone modifications.

In conclusion, we have demonstrated that chromatin modifications function as important determinants of 3D genome architecture, particularly for the formation of genome compartments and TADs. Our studies open new directions for understanding the mechanisms underlying 3D genome architecture in metazoans and the consequent regulation of genome functions.

Materials and Methods

Detailed materials and methods are available in *SI Appendix, SI Methods and Methods*.

Strains. *C. elegans* strains used in this study include: N2 Bristol strain (wild-type), RB2301 *cec-4(ok3124)* IV, and GW0638 *met-2(n4256) set-25(n5021)* III. All strains were maintained at 20 °C on NGM plates seeded with OP50 grown in LB.

Hi-C and Data Analysis. The in situ Hi-C protocol was performed on mixed-stage mutant embryos of genotypes *cec-4* (two biological replicates) and *met-2 set-25* (three biological replicates), as described previously (41). Hi-C data analyses were performed using scripts derived from hiclib and cworld packages (40, 41) (*SI Appendix*). Comparisons were made to our Hi-C data (10) from wild-type embryos (GSM3680067 in the National Center for Biotechnology Information Gene Expression Omnibus [GEO]: accession no. GSE128568).

ChIP-Seq and Data Analysis. SDC-3 ChIP-seq was performed on mixed-stage mutant embryos of genotypes *met-2 set-25* (two biological replicates) and *cec-4* (one biological replicate) as described in *SI Appendix*. SDC3 ChIP-seq datasets from this study, and from published SDC-3 ChIP-seq datasets downloaded from GEO (accession no. GSE122639) (43), were analyzed as in ref. 10. Previously published early-embryo H3K9me2 and H3K9me3 ChIP-seq datasets (accession no. SRP080806), L1 larvae H3K9me2 ChIP-seq datasets (accession no. GSE126884), and early-embryo H3K9me1, H3K9me2, and H3K9me3 ChIP-chip datasets (accession nos. GSE22720, GSE22740, and GSE22746) were downloaded from the Sequence Read Archive (SRA) and GEO and reanalyzed (*SI Appendix*).

RNA-Seq Data Analysis. RNA-seq data from N2, *cec-4*, and *met-2 set-25* early embryos (accession no. GSE74134) (36) and L1 larvae (accession no. GSE79597) (44) were downloaded from the GEO and analyzed using the DESeq2 package in R (*SI Appendix*).

Data Availability. Hi-C and ChIP-seq datasets from this study are available through GEO accession no. GSE144253 (63).

ACKNOWLEDGMENTS. We thank D. Stalford for graphic design and B.J.M. laboratory members for discussions. This work used the Vincent J. Coates Genomics Sequencing Laboratory at University of California, Berkeley, supported by NIH S10 OD018174 Instrumentation Grant. Q.B. is supported by The Program for Professor of Special Appointment (Eastern Scholar) at Shanghai Institutions of Higher Learning (TP2018044), the Shanghai Pujiang Program (18PJ1406800), and the National Natural Science Foundation of China (31801056 and 31970585). B.J.M. is an investigator of the Howard Hughes Medical Institute and received funding via NIH Grants R01GM30702 and R35GM131845.

1. W. A. Bickmore, B. van Steensel, Genome architecture: Domain organization of interphase chromosomes. *Cell* **152**, 1270–1284 (2013).
2. B. Bonev, G. Cavalli, Organization and function of the 3D genome. *Nat. Rev. Genet.* **17**, 661–678 (2016).
3. L. A. Mirny, M. Imakaev, N. Abdennur, Two major mechanisms of chromosome organization. *Curr. Opin. Cell Biol.* **58**, 142–152 (2019).
4. A. Sanyal, B. R. Lajoie, G. Jain, J. Dekker, The long-range interaction landscape of gene promoters. *Nature* **489**, 109–113 (2012).
5. S. S. P. Rao *et al*., A 3D map of the human genome at kilobase resolution reveals principles of chromatin looping. *Cell* **159**, 1665–1680 (2014).
6. J. R. Dixon *et al*., Topological domains in mammalian genomes identified by analysis of chromatin interactions. *Nature* **485**, 376–380 (2012).
7. E. P. Nora *et al*., Spatial partitioning of the regulatory landscape of the X-inactivation centre. *Nature* **485**, 381–385 (2012).
8. M. I. Robson, A. R. Ringel, S. Mundlos, Regulatory landscaping: How enhancer-promoter communication is sculpted in 3D. *Mol. Cell* **74**, 1110–1122 (2019).
9. J. A. Beagan, J. E. Phillips-Cremins, On the existence and functionality of topologically associating domains. *Nat. Genet.* **52**, 8–16 (2020).
10. E. C. Anderson *et al*., X chromosome domain architecture regulates Caenorhabditis elegans lifespan but not dosage compensation. *Dev. Cell* **51**, 192–207.e6 (2019).
11. I. Williamson *et al*., Developmentally regulated *Shh* expression is robust to TAD perturbations. *Development* **146**, dev179523 (2019).
12. D. G. Lupiáñez *et al*., Disruptions of topological chromatin domains cause pathogenic rewiring of gene-enhancer interactions. *Cell* **161**, 1012–1025 (2015).
13. M. Franke *et al*., Formation of new chromatin domains determines pathogenicity of genomic duplications. *Nature* **538**, 265–269 (2016).
14. A. Despang *et al*., Functional dissection of the Sox9-Kcnj2 locus identifies nonessential and instructive roles of TAD architecture. *Nat. Genet.* **51**, 1263–1271 (2019).
15. E. Lieberman-Aiden *et al*., Comprehensive mapping of long-range interactions reveals folding principles of the human genome. *Science* **326**, 289–293 (2009).
16. E. P. Nora *et al*., Targeted degradation of CTCF decouples local insulation of chromosome domains from genomic compartmentalization. *Cell* **169**, 930–944.e22 (2017).
17. S. S. P. Rao *et al*., Cohesin loss eliminates all loop domains. *Cell* **171**, 305–320.e24 (2017).
18. W. Schwarzer *et al*., Two independent modes of chromatin organization revealed by cohesin removal. *Nature* **551**, 51–56 (2017).
19. G. Wutz *et al*., Topologically associating domains and chromatin loops depend on cohesin and are regulated by CTCF, WAPL, and PDS5 proteins. *EMBO J.* **36**, 3573–3599 (2017).
20. J. Nuebler, G. Fudenberg, M. Imakaev, N. Abdennur, L. A. Mirny, Chromatin organization by an interplay of loop extrusion and compartmental segregation. *Proc. Natl. Acad. Sci. U.S.A.* **115**, E6697–E6706 (2018).
21. M. J. Rowley *et al*., Evolutionarily conserved principles predict 3D chromatin organization. *Mol. Cell* **67**, 837–852.e7 (2017).
22. M. Falk *et al*., Heterochromatin drives compartmentalization of inverted and conventional nuclei. *Nature* **570**, 395–399 (2019).
23. A. G. Larson *et al*., Liquid droplet formation by HP1α suggests a role for phase separation in heterochromatin. *Nature* **547**, 236–240 (2017).
24. A. R. Strom *et al*., Phase separation drives heterochromatin domain formation. *Nature* **547**, 241–245 (2017).
25. Q. Bian, N. Khanna, J. Alvikas, A. S. Belmont, β-Globin *cis*-elements determine differential nuclear targeting through epigenetic modifications. *J. Cell Biol.* **203**, 767–783 (2013).
26. J. C. Harr *et al*., Directed targeting of chromatin to the nuclear lamina is mediated by chromatin state and A-type lamins. *J. Cell Biol.* **208**, 33–52 (2015).
27. B. D. Towbin *et al*., Step-wise methylation of histone H3K9 positions heterochromatin at the nuclear periphery. *Cell* **150**, 934–947 (2012).
28. D. O'Carroll *et al*., The polycomb-group gene Ezh2 is required for early mouse development. *Mol. Cell. Biol.* **21**, 4330–4336 (2001).
29. A. H. F. M. Peters *et al*., Loss of the Suv39h histone methyltransferases impairs mammalian heterochromatin and genome stability. *Cell* **107**, 323–337 (2001).
30. M. Tachibana *et al*., G9a histone methyltransferase plays a dominant role in euchromatic histone H3 lysine 9 methylation and is essential for early embryogenesis. *Genes Dev.* **16**, 1779–1791 (2002).
31. J. M. Galazka *et al*., Neurospora chromosomes are organized by blocks of importin alpha-dependent heterochromatin that are largely independent of H3K9me3. *Genome Res.* **26**, 1069–1080 (2016).
32. A. D. Klocko *et al*., Normal chromosome conformation depends on subtelomeric facultative heterochromatin in *Neurospora crassa*. *Proc. Natl. Acad. Sci. U.S.A.* **113**, 15048–15053 (2016).
33. J. Ahringer, S. M. Gasser, Repressive chromatin in *Caenorhabditis elegans*: Establishment, composition, and function. *Genetics* **208**, 491–511 (2018).
34. T. Liu *et al*., Broad chromosomal domains of histone modification patterns in *C. elegans*. *Genome Res.* **21**, 227–236 (2011).
35. K. Ikegami, T. A. Egelhofer, S. Strome, J. D. Lieb, Caenorhabditis elegans chromosome arms are anchored to the nuclear membrane via discontinuous association with LEM-2. *Genome Biol.* **11**, R120 (2010).
36. A. Gonzalez-Sandoval *et al*., Perinuclear anchoring of H3K9-methylated chromatin stabilizes induced cell fate in *C. elegans* embryos. *Cell* **163**, 1333–1347 (2015).
37. P. Zeller *et al*., Histone H3K9 methylation is dispensable for *Caenorhabditis elegans* development but suppresses RNA:DNA hybrid-associated repeat instability. *Nat. Genet.* **48**, 1385–1395 (2016).
38. J. Padeken *et al*., Synergistic lethality between BRCA1 and H3K9me2 loss reflects satellite derepression. *Genes Dev.* **33**, 436–451 (2019).
39. C. E. Delaney *et al*., Heterochromatic foci and transcriptional repression by an unstructured MET-2/SETDB1 co-factor LIN-65. *J. Cell Biol.* **218**, 820–838 (2019).
40. E. Crane *et al*., Condensin-driven remodelling of X chromosome topology during dosage compensation. *Nature* **523**, 240–244 (2015).
41. K. Brejc *et al*., Dynamic control of X chromosome conformation and repression by a histone H4K20 demethylase. *Cell* **171**, 85–102.e23 (2017).
42. Q. Bian, E. C. Anderson, K. Brejc, B. J. Meyer, Dynamic control of chromosome topology and gene expression by a chromatin modification. *Cold Spring Harb. Symp. Quant. Biol.* **82**, 279–291 (2017).
43. L. A. Street *et al*., Binding of an *X*-specific condensin correlates with a reduction in active histone modifications at gene regulatory elements. *Genetics* **212**, 729–742 (2019).
44. M. J. Snyder *et al*., Anchoring of heterochromatin to the nuclear lamina reinforces dosage compensation-mediated gene repression. *PLoS Genet.* **12**, e1006341 (2016).
45. A. W. Snowden, P. D. Gregory, C. C. Case, C. O. Pabo, Gene-specific targeting of H3K9 methylation is sufficient for initiating repression in vivo. *Curr. Biol.* **12**, 2159–2166 (2002).
46. A. Rechtsteiner *et al*., Repression of germline genes in *Caenorhabditis elegans* somatic tissues by H3K9 dimethylation of their promoters. *Genetics* **212**, 125–140 (2019).
47. M. Di Pierro, R. R. Cheng, E. Lieberman Aiden, P. G. Wolynes, J. N. Onuchic, De novo prediction of human chromosome structures: Epigenetic marking patterns encode genome architecture. *Proc. Natl. Acad. Sci. U.S.A.* **114**, 12126–12131 (2017).
48. Y. Qi, B. Zhang, Predicting three-dimensional genome organization with chromatin states. *PLOS Comput. Biol.* **15**, e1007024 (2019).
49. A. N. Sawh *et al*., Lamina-dependent stretching and unconventional chromosome compartments in early *C. elegans* embryos. *Mol. Cell* **78**, 96–111.e6 (2020).
50. M. J. Rowley *et al*., Condensin II counteracts cohesin and RNA polymerase II in the establishment of 3D chromatin organization. *Cell Rep.* **26**, 2890–2903.e3 (2019).
51. X. Zheng *et al*., Lamins organize the global three-dimensional genome from the nuclear periphery. *Mol. Cell* **71**, 802–815.e7 (2018).
52. S. V. Ulianov *et al*., Nuclear lamina integrity is required for proper spatial organization of chromatin in Drosophila. *Nat. Commun.* **10**, 1176 (2019).
53. L. J. Barton, A. A. Soshnev, P. K. Geyer, Networking in the nucleus: A spotlight on LEM-domain proteins. *Curr. Opin. Cell Biol.* **34**, 1–8 (2015).
54. J. R. Dixon *et al*., Chromatin architecture reorganization during stem cell differentiation. *Nature* **518**, 331–336 (2015).
55. B. Bonev *et al*., Multiscale 3D genome rewiring during mouse neural development. *Cell* **171**, 557–572.e24 (2017).
56. J. Ray, *et al*., Chromatin conformation remains stable upon extensive transcriptional changes driven by heat shock. *Proc. Natl. Acad. Sci. U.S.A.* **116**, 19431–19439 (2019)
57. H. P. Cam *et al*., Comprehensive analysis of heterochromatin- and RNAi-mediated epigenetic control of the fission yeast genome. *Nat. Genet.* **37**, 809–819 (2005).
58. J. G. Wood *et al*., Chromatin-modifying genetic interventions suppress age-associated transposable element activation and extend life span in Drosophila. *Proc. Natl. Acad. Sci. U.S.A.* **113**, 11277–11282 (2016).
59. A. Bulut-Karslioglu *et al*., Suv39h-dependent H3K9me3 marks intact retrotransposons and silences LINE elements in mouse embryonic stem cells. *Mol. Cell* **55**, 277–290 (2014).
60. G. Fudenberg *et al*., formation of chromosomal domains by loop extrusion. *Cell Rep.* **15**, 2038–2049 (2016).
61. A. L. Sanborn *et al*., Chromatin extrusion explains key features of loop and domain formation in wild-type and engineered genomes. *Proc. Natl. Acad. Sci. U.S.A.* **112**, E6456–E6465 (2015).
62. W. A. Flavahan *et al*., Insulator dysfunction and oncogene activation in IDH mutant gliomas. *Nature* **529**, 110–114 (2016).
63. B. J. Meyer *et al*., Histone H3K9 methylation promotes formation of genome compartments in *C. elegans* via chromosome compaction and perinuclear anchoring. Gene Expression Omnibus. https://www.ncbi.nlm.nih.gov/geo/query/acc.cgi?acc=GSE144253. Deposited 25 January 2020.